Author Manuscript

Emergent Properties, Functions, and Applications of Phane-based Polymers

John Kim[†], Arit Patra[†], Soumyamouli Pal[†], Nicholas L. Abbott, Joerg Lahann**

J. Kim, A. Patra, Prof. J. Lahann

Biointerfaces Institutes, University of Michigan, 2800 Plymouth Road, Ann Arbor, MI 48109, USA
E-mail: lahann@umich.edu

J. Kim, Prof. J. Lahann
Department of Materials Science and Engineering, University of Michigan, 2300 Hayward Street, Ann Arbor, MI 48109, USA

A. Patra, Prof. J. Lahann

Department of Chemical Engineering, University of Michigan, 2300 Hayward Street, Ann Arbor, MI 48109, USA

Soumyamouli Pal, Prof. Nicholas L. Abbott

Smith School of Chemical and Biomolecular Engineering, Cornell University, Ithaca, NY 14853, USA

[†]These authors contributed equally: John Kim, Arit Patra, Soumyamouli Pal

Keywords: Chemical vapor deposition, paracyclophane, organic field electric transistor, biomolecule immobilization, membrane, liquid crystal, nanostructures

Abstract: Over the past few decades, chemical vapor deposition (CVD) of [2.2]paracyclophanes has captured significant attention as an emergent technology, producing conformal, chemically pure, and pinhole-free coatings for biomedical and industrial applications. Compelling examples range from functional CVD polymers to tailored nanostructures. In this manuscript, we connect the unique functional properties of polymers derived from [2.2]paracyclophanes with emergent applications. We specifically focus on function-property relationships in the areas of electronic materials,

This is the author manuscript accepted for publication and has undergone full peer review but has not been through the copyediting, typesetting, pagination and proofreading process, which may lead to differences between this version and the Version of Record. Please cite this article as doi: 10.1002/adfm.202315891.

This article is protected by copyright. All rights reserved.

Author Manuscript

biomaterials, and separation materials. A particular focus is to highlight the versatility of Chemical Vapor Deposition Polymerization to process these polymers.

1. Introduction

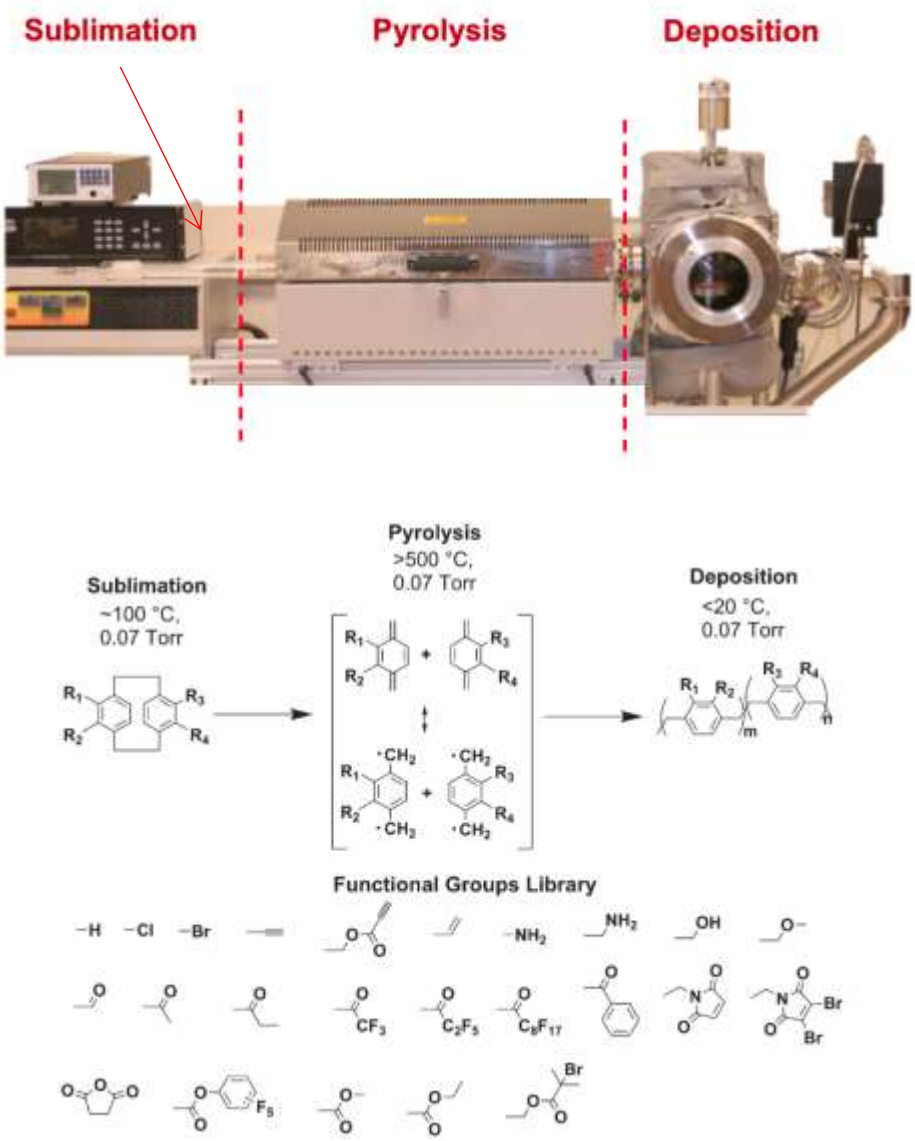


Figure 1. Digital image of a CVD installation that is used to prepare reactive coatings based on functionalized poly(p-xylylene)s. Precursors vaporize in the sublimation zone and are transferred to the pyrolysis zone where reactive species are formed. Subsequently, precursors enter the reaction chamber and polymerize on

This article is protected by copyright. All rights reserved.

Author Manuscript

a cooled stage. Reaction scheme of the CVD polymerization of functionalized PCPs. Reproduced with permission. [22] Copyright 2006, Wiley-VCH, [5] copyright 2017, Wiley-VCH.

For many applications, conventional wet chemical coating processes, such as spray and paint coating, dip coating, or spin coating offer good functional outcomes. However, if precise control of thicknesses, high coating quality, and conformal coating of complex geometries are required, wet chemical processes have severe limitations that can be addressed by CVD polymerization: (1) During the drying and baking step of wet chemical processes, the solvent evaporates and simultaneously creates pores and cracks in the polymer coating, degrading the material quality. (2) Solvent-based coating processes depend on the substrate surface energy. Also, solvent compatibility of the substrate plays a key factor in these processes so that the substrate does not corrode when in contact with the solvent. (3) Topographically porous surfaces and curved geometries are very difficult to coat using wet chemical processes and usually require multi-step processing. Over the past few decades, chemical vapor deposition (CVD) has captured significant attention as an emergent technology, producing conformal, chemically pure, and pinhole-free coatings for biomedical and industrial applications.[1--5] Physical vapor deposition (PVD), such as electron-beam evaporation, can effectively control the thickness of coating layers ranging from nanometers to microns, but it is challenging to uniformly coat complex surfaces due to limited conformality. Similar to atomic layer deposition (ALD), CVD polymerization can yield nanometer-thin layers of pinhole-free coatings. Furthermore, CVD polymerization tends to result in chemically stable polymers with very high molecular weights that show excellent chemical tunability, insulating properties, and mechanical stability.[1],[5],[6],[7] In general, CVD processes offer fast and scalable solutions if high-quality films with controlled thicknesses are required. CVD processing is compatible with a wide range of reaction mechanisms, such as metal-organic CVD, plasma-enhanced CVD, initiated CVD, and oxidative CVD.[6,8--14] To date, the most widely utilized CVD process for producing polymers is based on CVD polymerization of [2.2]paracyclophanes precursors (PCPs), which results in high-molecular-weight, linear polymers, i.e., poly(*p*-xylylene) (PPX).[3] Following Szwarc's initial discovery of PPX polymerization from p-xylene, Gorham devised an efficient pathway, often called the Gorham process, employing chemical vapor deposition polymerization to deposit PPX films. [3,15,16] In the

This article is protected by copyright. All rights reserved.

Author Manuscript

Gorham process, the precursor molecule, almost always a [2,2]paracyclophane (PCP) derivative, is sublimed at a temperature around 100--200 °C and a working pressure of 0.1-0.4 mbar. The precursor is then transferred into the pyrolysis zone, where it undergoes homolysis at 550--650 °C to form reactive dimers, *p*-quinodimethanes, that can exist in either triplet or singlet states.[17] Finally, the *p*-quinodimethanes are transferred onto a solid substrate, where they undergo spontaneous polymerization. Deposition rates during the CVD process generally range approximately from 0.01 nm/s to 0.04 nm/s as measured by a quartz crystal microbalance (QCM). The thickness control can be augmented by the use of an inert carrier gas, such as argon. In this case, the deposition rate can be controlled in real-time through the feedback loop between the flow controller, a valve controlling the working pressure, and the QCM sensor. The sublimation rate also can be varied by changing the temperature of the monomer boat which can control the deposition rate. Due to the constraint of being a vacuum process, CVD polymerization is typically run as batch or semi-continuous processes, including roll-to-roll processing.[18]

In general, PPX films exhibit excellent mechanical properties, inertness to organic solvents, and thermal stability.[11,12] The base PPX polymer, also known as Parylene™, has demonstrated its industrial potential in a variety of applications, including field-electric transistors as a passive layer,[19,20] microelectromechanical systems,[21] biomedical devices, and bioresponsive surfaces.[22] This review will provide representative examples of functional CVD polymers with applications ranging from conventional thin films to tailored nanostructures.

2. Application of PPXs as gate dielectric material for thin-film transistors (TFTs)

The dielectric layer in insulated-gate field-effect transistors (IGFETs) plays a key role in the device operation since the applied gate voltage polarizes the dielectric layer which leads to charge carrier mobility in the semiconductor channel. Intrinsic properties of the dielectric layer, such as its dielectric constant, as well as extrinsic properties like defects at the interface between the dielectric layer and the semiconductor layer, determine the performance of the IGFETs. Because of their relatively high electron mobility (Figure 1d) over a wide range of voltages and frequencies, and their pinhole-free conformal coating properties, PPX films have found applications as gate materials in IGFETs.[21,23] Generally, to induce a given number of charge carriers, a dielectric material with a

This article is protected by copyright. All rights reserved.

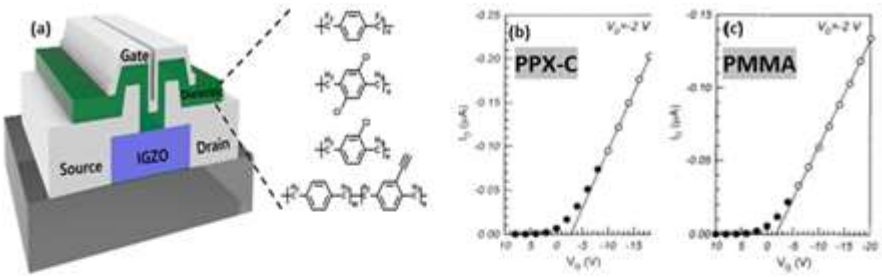
Author Manuscript

higher dielectric constant will require a lower gate voltage to be applied, enabling the fabrication of power-efficient devices. In terms of the extrinsic characteristics, which are highly dependent on the synthesis procedure of the dielectric layer, disorder at the interface between the dielectric and the channel layer can cause dangling bonds and charge trapping at the interface, resulting in lower mobility of charge carriers in the channel and lower on-state current. It can also lead to hysteresis in transfer characteristics and large subthreshold swings (SS). Therefore, the selection of an optimum dielectric material must consider its dielectric properties as well as the availability of appropriate and defect-free deposition methods.[24]

Dimitrakopoulos et al. proposed the use of PPX as polymeric gate insulator materials replacing conventional inorganic materials such as SiO_X and SiN_X.[25,26] Using dihexylsexithiophene (DH6T) as the semiconductor material, they compared the CVD polymer poly(4-chloro-p-xylylene) (PPX-C) with polymethyl methacrylate (PMMA) and polyimide as gate insulators. Among these polymers, PPX-C resulted in some of the highest field-effect mobility values among organic IGFETS materials, reported at the time, which were as high as 0.131 $cm^2 V^{-1} S^{-1}$.

This article is protected by copyright. All rights reserved.

Author Manuscript



(d)

Dielectric	Configuration	Semiconductor	Mobility ($cm^2 V^{-1} S^{-1}$)
PPX-C	SLGD	DH6T	0.131
PMMA	SLGD	DH6T	0.08
PPX-C	SLGD	IGZO	6.22
PPX-AF4	SLGD	IGZO	6.23
PPX-AF4	SLGD	BZTO	22.72
PPX-C/PPX-AF4	DLGD	TIPS - pentacene	0.13
PPX-C+PPX-AF4	DLGD with co-deposition	TIPS - pentacene	0.14

Figure 2: (a) PPX polymers used as dielectric films in TFT devices. Transfer characteristics (plot of ID vs VG) at VD = -2 V for (b) 370 nm thick PPX-C as gate insulator, (c) 1601 nm thick PMMA as gate insulator, higher slope from the plot signifies larger carrier mobility values; (d) Summary of mobility values for various dielectric chemistries, semiconductor materials, and device configurations (SLGD: single layer gate device; DLGD: double layer gate device). Reproduced with permission. [27] copyright 2021, American Chemical Society. [25] Copyright 1998, Elsevier.

Kim et al. recently improved upon previous studies by developing thin-film transistors comprised of a range of PPX derivatives as dielectrics for use with oxide-based semiconductors on flexible plastic substrates.[27] In these configurations, they observed the highest mobility values among organic TFTs, which were as high as 22.72 $cm^2 V^{-1} S^{-1}$. In this study, a 100 nm thick dielectric film of PPX with differing functional groups including PPX-C, poly(dichloro-p-xylylene) (PPX-D), and alkyl-functionalized poly(tetrafluoro-p-xylylene) (PPX-AF4) was used in combination with an In-Ga-Zn-O (IGZO) semiconductor. Their mobility values were 6.22, 5.81, and 6.23 $cm^2 V^{-1} S^{-1}$, respectively,

This article is protected by copyright. All rights reserved.

Author Manuscript

which favorably compared to conventional SiO_2 dielectric top gates. Alternatively, semiconductor-insulator TFT designs that feature barium zinc tin oxide (BZTO) as the semiconductor material have been explored. In this case, a 60 nm thick PPX-AF4 layer, a combination yielded the highest mobility values (Figure 2D). Notably, CVD polymerization of functionalized PCPs allows for precise fine-tuning of the dielectric constant, while providing chemical anchor groups for further surface modification. For example, organic dyes have been conjugated to TFTs via functional groups available on the PPX films.[28] This strategy can result in the fabrication of photosensitive TFT devices.

Double-layer gate dielectrics (DLGD) are excellent for tuning gate-source currents (I_{GS}) and threshold voltages (V_{TH}) in TFT devices, because they allow for independent control of each dielectric layer's frequency-response-related stability by varying the thickness ratio of dielectric layers.[29,30] Fukuda et al. explored DLGD configurations to suppress polarization effects due to the crystallinity of PPX-C by introducing a second dielectric layer of amorphous fluoropolymer PPX-AF4 which promotes interfacial charge trapping.[31] Park et al. demonstrated high-performance organic field-effect transistors (OFETs) consisting of DLGDs with PPX-C as the top layer, PPX-AF4 as the base layer, and 6,13-Bis(triisopropylsilylethynyl)pentacene (TIPS pentacene) as the semiconductor material.[32] For PPX-C single-layer configurations, they observed higher drain-source currents, smaller threshold voltages, and higher mobility than for otherwise identical PPX-AF4 configurations. However, PPX-AF4 can add additional features such as smaller gate-source currents and higher device electrical stability. In DLGD device configurations, the PPX-AF4 base layer contributes to enhanced charge transport, OFET operational stability, and improved electrical characteristics, even though it is not directly in contact with the organic semiconductor. It was reported that an optimized DLGD performance can be obtained with a PPX-C thickness ratio of 0.63.

In some contexts, the fabrication of DLGDs can be challenging, especially when one of the dielectric materials is not chemically or mechanically compatible with the semiconductor material. For example, Shin et al. reported that the PPX-C dielectric layer exhibits large gate leakage density, low breakdown voltage, and a degraded field effect mobility of 0.007 $cm^2\ V^{-1}\ S^{-1}$ in field-effect transistors with n-channel semiconductors.[32] Compelling X-ray photoelectron spectroscopy (XPS) results indicated that non-bonding electrons in the chlorine atoms of PPX-C reduced the strong electron withdrawing capacity of the poly{[*N*,*N*'-bis(2-octyldodecyl)-naphthalene-1,4,5,8-

This article is protected by copyright. All rights reserved.

Author Manuscript

bis(dicarboximide)-2,6-diyl]-*alt*-5,5'-(2,2'-bithiophene)} semiconductor layer, thereby degrading its electronic properties. However, when a very thin protective layer of PMMA or polystyrene (PS) was deposited in between the PPX-C and the semiconductor, the mobility significantly improved to 0.47 and 0.13 $cm^2 V^{-1} S^{-1}$, respectively, enabling stable and reliable device operation. Despite significant progress, there are still substantial drawbacks with DLGDs, as they require a multistep deposition process leading to additional cost and complexity related to the fabrication process. Park et al. demonstrated that sequential deposition of the two polymers PPX-C and PPX-AF4 using a two-stage temperature profile for the sublimation zone resulted in bilayer films.[33] These co-deposited dielectric layers exhibited improved electrical characteristics in comparison to the DLGDs; for DLGDs, mobility decreased, and threshold voltage increased with increasing PPX-AF4 weight fraction. However, for co-deposited gate dielectrics (CGDs), the electron mobility remained high and the threshold voltage remained low independent of the weight fraction of PPX-AF4. The fact that the CVD deposition can proceed at low temperatures and leads to polymer films with favorable mechanical properties makes this process well-suited for the functionalization of flexible plastic substrates. In general, PPX coatings exhibit excellent durability during bending, a feature that is critical for flexible electronics applications.[34]

3. Biomedical applications of PPXs

As the interest in advanced medical treatment techniques increase, such as artery stents, implants, bioadhesive sensors, and wound healing patches, demands for tailored biointerfaces are surging.[35--38] In this context, CVD polymerization offers great potential for improving the biocompatibility of medical devices.[22,38--45] Due to their high molecular weight, excellent adhesive properties, and conformal coverage, CVD polymers, including PPXs, have garnered great interest as drug-eluting stent (DES) coatings.[43] There has been remarkable progress in DES, such as a Food and Drug Administration (FDA)-approved product by Boston Scientific commercialized under the tradename Taxus.[46] Using functionalized PPX coatings, poly- (hydroxymethyl-*p*-xylylene-co-*p*-xylylene) (PPX-HM), Vorwerk et al. attempted to design biocompatible stents that do not require the release of therapeutic drugs.[43] They confirmed the *in vitro* biocompatibility of PPX-HM-coated stents based on a reduction in platelet adhesion compared to the uncoated controls. Also, thrombin-antithrombin complex generation was reduced by 40% for the PPX-HM-coated samples. Studies performed in vivo

This article is protected by copyright. All rights reserved.

Author Manuscript

have generally found low levels of thrombocyte adhesion and reduced occlusion for PPX-HM coated stents, while they also reported increased neointimal formation. However, it is important to note that these coatings were drug-free, and an anticoagulant was used throughout the study. To further improve the biocompatibility of PPX-coated stents, functionalization of the stent surface using chemically reactive PPX coatings for immobilization of biologics could be employed.

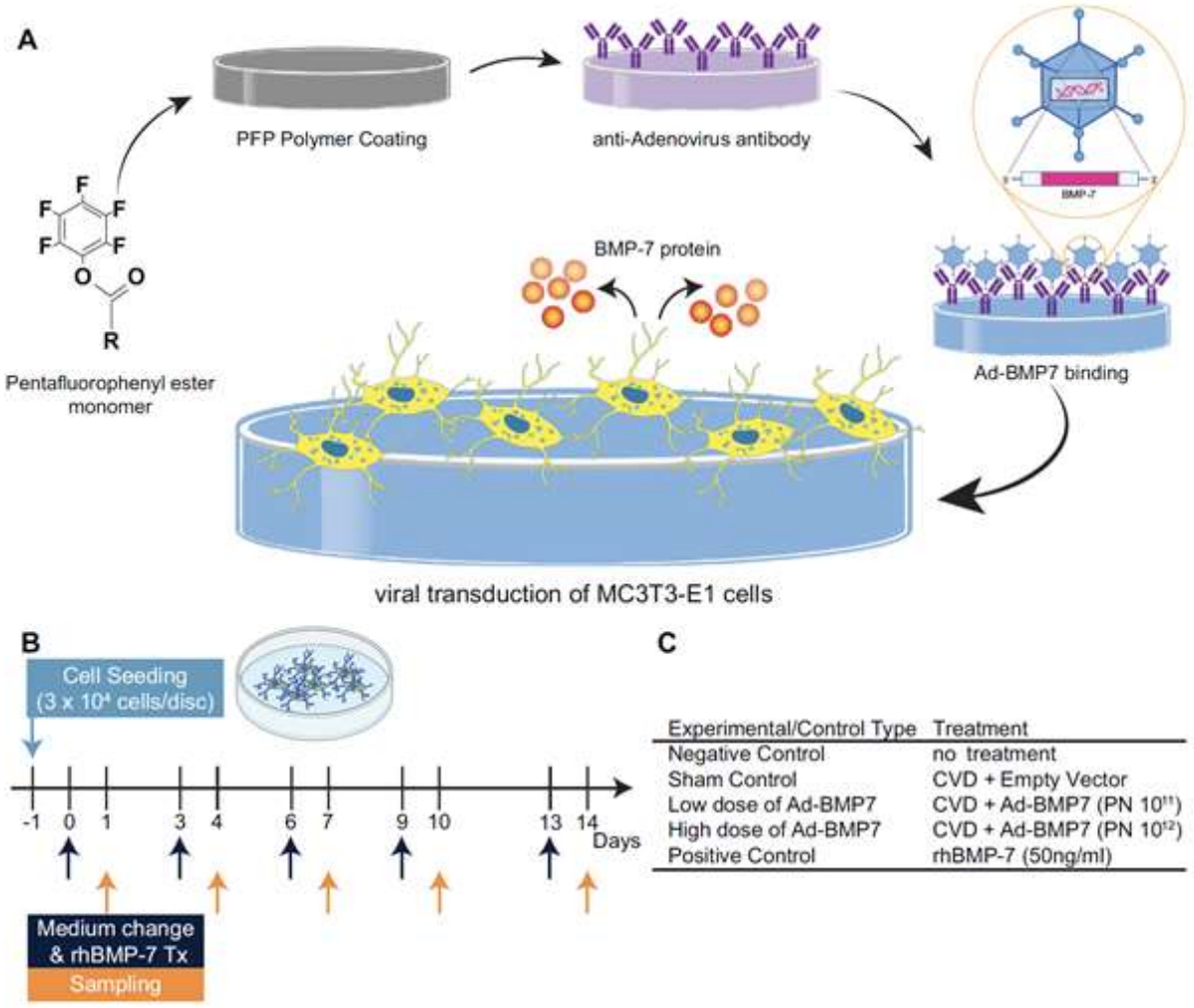


Figure 3. Experimental design of an in vitro study based on CVD polymeric films deposited onto titanium. A) Schematic rendering of chemical vapor deposition (CVD) polymerization depicting sublimation of the pentafluorophenyl (PFP) ester precursor, which forms a 17.3 ± 0.2 (mean ± SD) nm polymer coating on the titanium surface. Following incubation with an anti-adenovirus antibody (10 µg ml^{-1}) and BMP-7-encoding adenovirus (10^{11} PN), MC3T3-E1 cells (3 × 10^4 cells/disc) were added and incubated. B) The experimental timeline showing the time points for osteoblast-induction media changes and collection of the supernatant

This article is protected by copyright. All rights reserved.

samples for subsequent analyses. C) Table showing the experimental and control treatment groups. Reproduced with permission.[42] Copyright 2022, Wiley-VCH.

Reactive coatings that can be used for tailoring surfaces with desired biomolecules (e.g., proteins or nucleic acids) have the potential to enable applications, such as microarrays, drug delivery, biomimetic surfaces, or biomolecular electronics.[22,39,41,47,48] In some instances, physical adsorption of biomolecules via van der Waals interactions, hydrogen bonding, or hydrophobic interactions can be effective in immobilizing biomolecules onto polymer surfaces.[49--51] However, chemical immobilization via covalent bonds is generally more desirable, mainly because it tends to provide more stability and can be used for site-directed immobilization. Lahann et al. have explored the use of tailor-made CVD films for covalent immobilization of a range of biomolecules including polysaccharides, antibodies, gene encoding vectors, and enzymes.[39,40,44,47,48,52--54] To improve bone integration, CVD polymerization has been used to anchor adenovirus encoding for bone morphogenetic protein (Ad-BMP-7) to PPX-coated dental titanium implants.[42] In this case, surface immobilization was proven to be more efficient than non-bound delivery which could lead to particles being captured by the liver and lung.[55,56] Prior to the immobilization of Ad-BMP-7, the implant surface was coated with pentafluorophenyl (PFP)-ester-functionalized PPX. Then, the anti-adenovirus antibody was anchored via amide bonds formed between amino groups of the antibody and the PFP-ester moieties presented on the coated implant surface. Finally, Ad-BMP-7 was tethered to the PPX-coated TiO_2 surfaces via antibody-antigen interactions. This strategy resulted in a continuous increase in metabolic activity and higher expression of BMP-7. They further conducted *in vivo* experiments in rats to evaluate the efficacy of gene delivery using CVD-coated titanium implants. After applying standardized oral defects to bones, implant contact (BIC) and bone mineral density (BMD) were assessed via micro-computer tomography (CT). After day 21, both regenerated bone volume and BMD increased for the Ad-BMP7 treatment group, whereas the control group without viral vectors had only marginal bone growth. This report suggests that using CVD to tether viral vectors that encode for therapeutic proteins on titanium surfaces not only improves bone regeneration but also avoids the need for high doses of growth factors that have caused the failure of market-approved therapies in the past.[55,56]

This article is protected by copyright. All rights reserved.

Author Manuscript

Author Manuscript

4. Membrane Applications

Another important advantage of the CVD process is the high degree of conformality of the resulting polymer coatings even at sub-micron thicknesses. This feature is attractive for membrane technologies, as films with lower thicknesses tend to feature higher permeation rates. Similarly, controlling the microporosity of these films can enhance the selectivity of membranes.[57] Accordingly, Shii et al. demonstrated the deposition of defect-free microporous organic polymer nanofilms onto ultrafiltration membranes fabricated by CVD polymerization of PCP derivatives (Figure 4A) with polar substituents.[58] By introducing cross-linking points within PPX nanofilms using

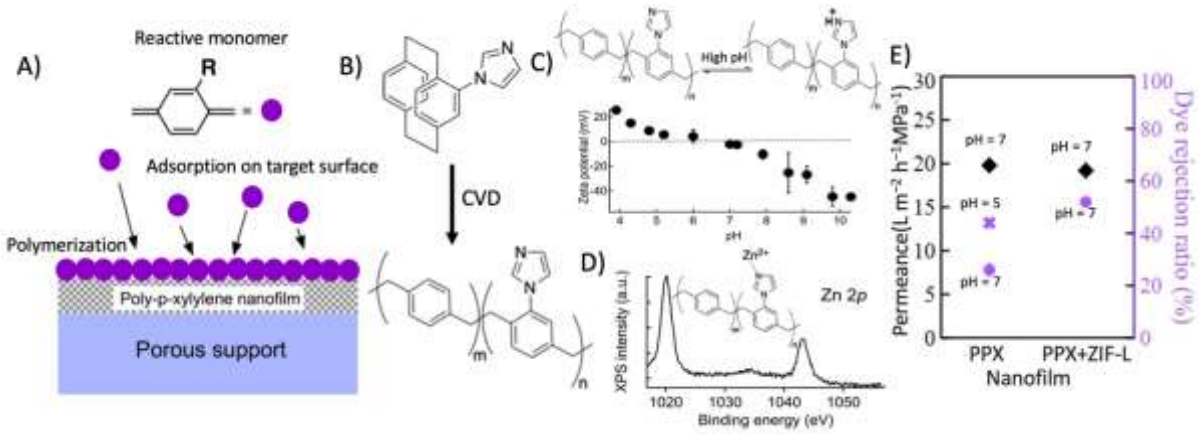


Figure 4. A) Schematic illustration of CVD of PPX films on porous supports. B) Molecular structure of the PCP used for CVD polymerization and the PPX film formed. C) Effect of pH on surface zeta potentials of the PCP film. D) Zn 2p XPS spectra of PCP film after treatment with an aqueous solution of $Zn(NO_3)_2 \cdot 6H_2O$ for 5 min. E) Water permeance and methylene blue dye rejection ratio of imidazole based PPX and ZIF-L PPX composite nanofilms. Reproduced with permission. [58] Copyright 2017, Nature Portfolio, [61] copyright 2023, MDPI.

a tailor-made PCP with a twisted biphenyl bridge, reduced polymer packing, improved water permeance, and high selectivity were achieved. The introduction of twisted crosslinking points into PPX led to enhanced microporosity as well as improved mechanical strength. The membranes coated with thin crosslinked microporous organic polymer nanofilms offer outstanding performance in terms of nanofiltration in water and alcohol. Blocking of the permeation of non-polar organic solvent through the nanofilms led to efficient recovery of water from an oil-water emulsion and thus has the potential to minimize chemical processes for oil recovery and water purification, a feature

This article is protected by copyright. All rights reserved.

Author Manuscript

that may also be of interest for pharmaceutical applications.[59,60] Since the free volume size within the membranes can be tuned by modifying substituents in PCP, robust and clean nanofilms fabricated by the CVD polymerization process have great potential to efficiently separate various target molecules.

Yoshida et al. further characterized the nanofiltration performance of PPX thin films possessing imidazole side chains prepared on the surface of commercial ultrafiltration membranes using a dry CVD process (Figure 4B).[61] The films showed an increase in rejection rates for the cationic dye and methylene blue (MB) due to the protonation of imidazole units below pH 7; amphoteric characteristics reflecting imidazolium cations and imidazoline anions at low and high pH ranges were observed (Figure 4C). Furthermore, the imidazole units could bind Zn^{2+} ions through coordination interactions enabling the direct growth of zeolitic imidazolate framework (ZIF) crystals on the surfaces of PPX films (Figure 4D). The resulting PPX+ZIF-L nanocomposite membranes displayed improved dye rejection rates for water-soluble organic dyes with increased water flux (Figure 4E). Well-defined and mechanically robust PPX films thus provide a platform for molecular separations through tuning free-volume sizes and specific interactions between their substituents and target solutes. Further studies are underway to establish the potential for various applications, such as an effective separation of biomolecules in biomedical devices and ultrathin ion-exchange membranes of energy storage devices.

5. Templated CVD polymerization leads to tailored nanostructures

This article is protected by copyright. All rights reserved.

Author Manuscript

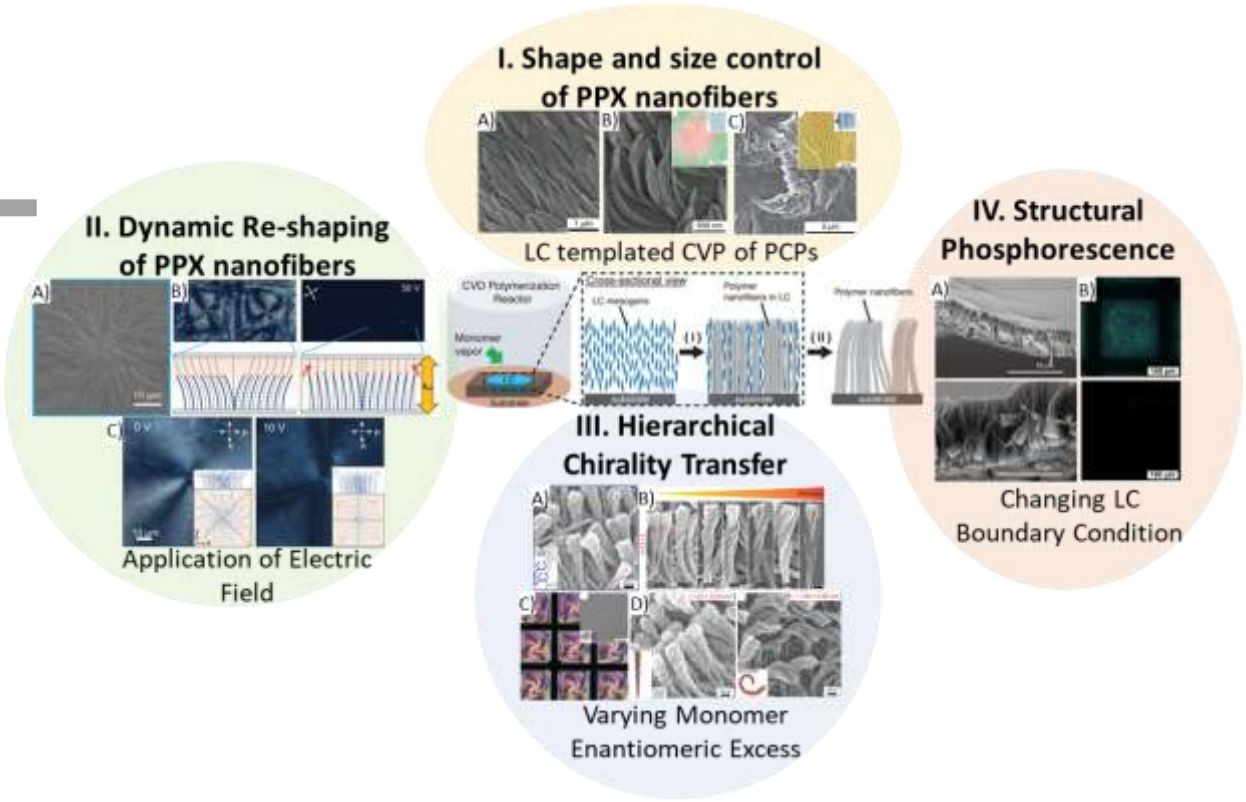


Figure 5. Schematic illustration of LC-templated CVD polymerization Ⅰ. LC-templated CVP of PCP-HM, (A-C) Scanning electron microscopy (SEM) images of nanofibers polymerized from PCP-HM (10 mg) in A) Nematic film of 5CB with homeotropic anchoring. B) Nematic film of E7 with hybrid anchoring C) E7 containing right-handed (R-811) dopants. II. Dynamic reshaping of PCP-HM nanofibers: A) Scanning electron micrographs of a nanofiber forest after removal of the PCH phase. B) Optical micrographs (cross polars) and corresponding side-view schematic illustrations of nanofibers in PCH after CVP in contact with H-PI-coated ITO glass without (left) and under an electric field (50 V/1 kHz, sine wave) (right). C) Changes in the optical appearance of a nanofiber-embedded LC under 0V (left) and 10V (right) at 1 kHz (sine waveform, thickness ≈100 μm). Insets show schematic illustration of the side-view (bottom) and top-view (top) of the nanofiber organizations. III. Hierarchical chirality transfer: A) SEM image of nanohelices prepared by CVD polymerization (the LC was homeotropically anchored on a surface before polymerization and was removed prior to SEM). B) SEM images of representative nanohelices prepared with varying enantiomeric excess. The scale bar represents 200 nm. C) POM image of LC phase after CVD polymerization of nanohelices displaying anti-clockwise patterns with its corresponding SEM image (inset). IV. Structural phosphorescence: A) SEM images of the lateral organized free-standing nanofiber membranes. B) Phosphorescence images of the nanofiber (top) and bulk films (bottom) of PCP-CH_2NH_2. Reproduced with permission. [63] Copyright 2018, American Association for the Advancement of Science, [70] copyright 2022, Wiley-VCH, [81] copyright 2022, Wiley-VCH, [90] copyright 2023, American Chemical Society.

Past studies, as described above, used CVD to form continuous PPX films.[62] Alternatively, CVD polymerization of PCPs, when performed into anisotropic templating phases such as liquid crystals (LCs), can also result in surface-attached ordered arrays of nanofibers.[63] This observation hints at a

This article is protected by copyright. All rights reserved.

Author Manuscript

range of possible future functional materials, as organized arrays of synthetic fibers have found broad technological applications ranging from filtration membranes and insulating coatings to tissue engineering scaffolds.[64--66] Specifically, Cheng et al. found that CVD of substituted and unsubstituted PCP into micrometer-thick films of nematic LCs supported on solid substrates resulted in the formation of surfaces decorated with ordered arrays of end-attached nanofibers.[63] The alignment of the nanofibers closely followed the orientation of the LC mesogens. For instance, CVD polymerization of PCP-HM into a film of nematic LC, 4-cyano-4'-pentylbiphenyl (5CB), supported on a silane-functionalized surface on which the LC mesogens are oriented perpendicular to the substrate, led to the formation of nanofibers that were straight and aligned perpendicular to the bottom surface (Figure 5I.A). The nanofibers adhered strongly to the surface and optical characterization revealed them to be birefringent with the refractive index being maximum along the fiber axis. These results indicate the alignment of polymer chains along the main axis of the nanofibers.[67] Importantly, the shapes of the nanofibers can be controlled by programming the orientations of LC mesogens. For example, the CVD of PCPs into a film of nematic 5CB with planar and homeotropic anchoring at the bottom and top LC surfaces, respectively, led to banana-shaped nanofibers (Figure 5I,B). Smectic LCs, with a statistical layering of oriented molecules, templated straight nanofibers with broadened tips arranged in conical fanlike morphologies and chiral nematic phases (cholesteric) yielded shape-controlled and chiral nanofiber assemblies with micrometer scale periodicities along with an organization consistent with the fingerprint pattern characteristic of cholesteric films (Figure 5I.C). Finally, complex 3-dimensional nanofiber organizations were obtained in cases where defect-rich blue-phase LCs were used as the templating medium. Significantly, the use of LCs as templates for CVD imparted a high level of control over the nanofiber length and diameter in addition to their shape. The length of the nanofibers is limited by the thickness of the LC film chosen and the diameter of the nanofibers is controlled by the extrapolation length of the LC template (Figure 5I.D).

Fibers embedded in soft matrices also provide crucial functions in biological systems through shape-coded actuation, for example in cytoskeletal control of cell shape.[68,69] The mechanical coupling of the end-attached PPX nanofibers with the LC template was studied by Roh et al.[70] They demonstrated that the LC template can be exploited not only for the synthesis of the nanofibers but

This article is protected by copyright. All rights reserved.

Author Manuscript

also for dynamic reshaping of the fibers (post-synthesis) through reorientation of the LC, leading to the emergence of unique programmable electro-optic responses. Specifically, they fabricated bent PPX-HM nanofibers via CVD polymerization (Figure 5II.A) into a LC mixture comprising 65 mol% 4-(trans-4-pentylcyclohexyl) benzonitrile (PCH 5) and 35 mol% 4-(trans-4-propylcyclohexyl) benzonitrile (PCH 3), an LC phase that assumes a tilted orientation at the free surface of the LC film and a perpendicular orientation at the chemically functionalized surface of the support solid surface.[71] An increase in optical retardance after CVD polymerization reveals that the PCH template undergoes a substantial reorganization during the synthesis of the nanofibers. Significantly, they showed that the bent nanofibers can be reshaped by an elastic torque transmitted from the LC using an electric field (Figure 5II.B and 5II.C). These composite LC-nanofiber films prepared by LC-templated CVD display emergent optical properties (Figure 5II.C) that are promising as the basis of advanced light valves and optical tweezers based on vortex light beams.[72,73]

Surfaces with mesoscale chirality are central to a range of emerging fields, including photonics, electronics,[74--76] chiral recognition,[77,78] biocompatible cell scaffolds,[66] or asymmetric crystallization.[79,80] Varadharajan et al. explored the synthesis and polymerization of chiral PCPs via LC-templated CVD polymerization, resulting in the formation of surfaces with enantiomorphically pure nanohelices when using an achiral nematic LC template.[81] Interestingly, the molecular chirality of the precursor defined the nanoscale features of the templated nanohelices, which in turn adopted mesoscale twist patterns in arrays of nanofibers that extended over hundreds of micrometers. Specifically, CVD polymerization of chiral precursors (S_p,S)-1-(4-[2.2]paracyclophanyl)ethanol and (S_p,R)-1-(4-[2.2]paracyclophanyl)ethanol into a 10--12 µm thick film of a nematic LC phase (E7), which aligned homeotropically on a surface resulted in regular arrays of nanohelices with exclusively counter-clockwise or clockwise twists depending on the molecular handedness of the precursor (Figure 5III. A). Interestingly, the observed nanohelix lengths were shorter than the LC film thickness and also significantly shorter than achiral nanofibers prepared by templated CVD polymerization.[63] However, the contour length of one turn of the nanohelices was found to be in good agreement with the LC film thicknesses used for experiments, corroborating previous findings that the thickness of the templating LC constitutes an upper limit for the length of the nanofibers.[63] The pitches of the nanohelices could be controlled via

This article is protected by copyright. All rights reserved.

Author Manuscript

copolymerization of achiral (PCP-HM) and chiral precursors during templated CVD polymerization. While 90% 1S + 10% PCP-HM mixture had a pitch of 160 ± 12 nm, further addition of the achiral precursor resulted in a significantly larger pitch. For example, the pitch of a mixture of 20% chiral precursor and 80% achiral PCP-HM was 604 ± 48 nm. Additionally, the pitch increased from 191 ± 21 nm to 743 ± 52 nm as the enantiomeric excess decreased from 80% to 10% (Figure 5III.B). Moreover, CVD polymerization of chiral precursors also resulted in higher-order arrangements of the nanohelices in the form of microscopic surface arrays, which was also corroborated by the emergence of characteristic twist patterns in the polarized optical images before the removal of the LC (Figure 5III.C). In addition, they also demonstrated the influence of chiral LC templates on mesoscale chiral information transfer to the nanohelices. When a nematic LC was replaced with a cholesteric LC, the nanohelices displayed morphologies commensurate with synergistic or competing effects depending on the chirality of precursors and LCs. For instance, precursors and LCs with the same chirality led to highly twisted nanohelices. On the other hand, the use of precursors and LCs with opposite handedness yielded relatively straight nanohelices because of their opposing chirality (Figure 5III.D). This interplay of LC and CVD polymerization precursor chirality enables a wide spectrum of manufacturing approaches for nanostructured polymeric films, which offer a remarkable level of control over the chirality of the nanostructures, with potential applications in sensing (amplification of weak chiral signatures) and chiral separations.

Table 1. Comparison of fabrication techniques to engineer fibrous structures.

	Scale	Material	Process complexity	Morphologies
Electrospinning [82,83]	nm to µm	Thermoplastic polymers	Few minutes	Fibrous sheet with patterns
Hydrothermal growth[84,85]	nm to µm	Quartz, oxides, tungstates, etc.	Hours to days	Nanorods

This article is protected by copyright. All rights reserved.

Author Manuscript

Extrusion[86,87]	cm to m	Thermoplastics, metals, alloy	Seconds to minutes	Various shape of cross-sections
LC-templated CVD[63,70,81]	nm	Phan-based polymers	Few minutes	End-attached nanofibers

Another property that can be utilized in a range of optoelectronic or bioimaging applications is the photophysical response of solid-state organic compounds that exhibit luminescence.[88,89] Wawryszyn et al. demonstrated the synthesis of free-standing arrays of laterally organized nanofibers prepared via LC-templated CVD polymerization which possess structurally emergent phosphorescence that is not observed in bulk films of identical chemical compositions.[90] In brief, they created freely suspended films of nematic LC E7, with homeotropic alignment and used them as templates for CVD polymerization of aminomethyl-[2.2]paracyclophane (PCP-AM). They discovered that this experimental geometry (a change in boundary conditions for the LC film as compared to the previous examples) led to the formation of free-standing polymer membranes comprised of hourglass-shaped fibers that were laterally aligned (Figure 5IV.A). The biconical fibers exhibited end diameters of 184 ± 74 nm, central minimum diameters of 68 ± 23 nm, and total fiber lengths of 4.1 ± 0.4 μm. Surprisingly, these nanofiber membranes were found to exhibit both short-lived and long-lived structural luminescence after optical excitation (Figure 5IV.B-D). This finding constitutes the first report of long-lived emission from solid-state PPX nanofibers. Potential applications of photoluminescent polymer arrays include organic sensors and optoelectronic devices.[91--93]

This article is protected by copyright. All rights reserved.

Author Manuscript

Not surprisingly, templated CVD polymerization has been contemplated as an attractive strategy to expand the synthesis of 2-dimensional biointerfaces for 3-dimensional cell culturing systems. For instance, Chen et al. introduced ice templates pre-loaded with cells and bioactive factors in the reaction chamber.[94,95] During the CVD polymerization process,

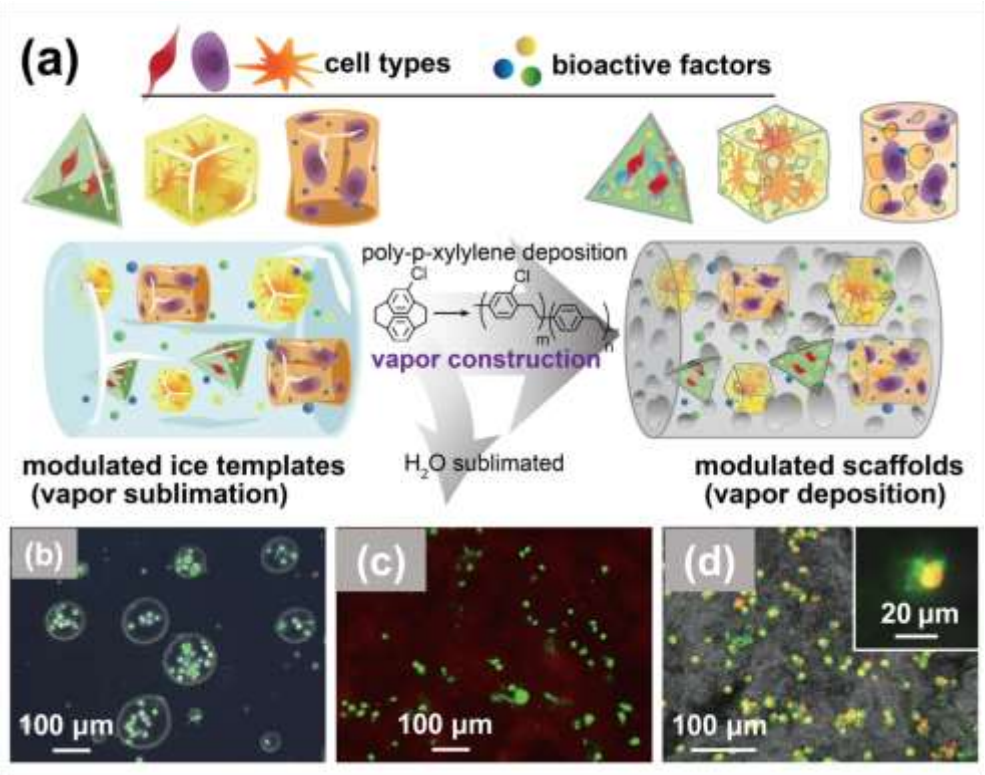


Figure 6. Fabrication of cell-laden and multifunctional scaffold modules. (a) Schematic illustration of vapor-phase sublimation and deposition fabrication process. Iced template modules with defined internal composition and outer architecture were formed through discrete module assembly and resulted in a continuous final modulated construct by subsequent vapor deposition. (b) An overlaid image of LIVE/DEAD-stained hASCs prepared in an oil-in-water system. Verification of hASCs within a fabricated module after vapor-phase deposition process by (c) LIVE/DEAD staining, (d) fluorescence labeling with Alexa Fluor 488-conjugated phallodin to stain the cytoskeleton (green) and propidium iodide to stain the nucleus (red); a high-resolution and magnified image of a stained cell was shown in the inset. Each experiment was repeated three times independently (n=3) with similar results. Reproduced with permission. [95] Copyright 2021,

they controlled the mass transport of precursors and sublimation of ice so that polymerization occurs on the template as it sublimes. As a result, they obtained porous cell-laden nanostructures. In their experiment, different types of live cells, buffers, and corresponding growth factors were impregnated in ice templates. They were able to preload

This article is protected by copyright. All rights reserved.

Author Manuscript

biomaterials into the ice templates and conduct CVD polymerization to obtain PPX scaffolds with volumes of ~5 cm^3 via control of the deposition time. The resulting cell-laden scaffolds exhibited a porosity of 63.4% ± 6.3 and a Young's modulus of 150 ± 21.5 kPa. After polymerization, they transferred the cell-laden samples to cell culture media to confirm the cell viability after CVD polymerization (via LIVE/DEAD staining and fluorescence labeling, Figure 6b, c). By comparing LIVE/DEAD signals, cell viability was confirmed to be 80.8% after the CVD polymerization. Additionally, they assessed the proliferation of human adipose-derived stem cells (hASCs) relative to control samples without the growth factor proteins. They confirmed the successful proliferation of hASC-derived cells and the existence of cytoskeleton within the CVD polymerized scaffold using fluorescence microscopy (Figure 6c, d). Furthermore, they assembled two ice templates loaded with different cells and biomolecules in various configurations to demonstrate the co-culturing of the cells. Overall, ice-templated CVD polymerization enables the fabrication of complex scaffolds for cell culture.

Although LC-templated CVD polymerization has yielded a range of continuous micro/nanostructures, it has so-far provided limited access to the synthesis of particles and their precise control of porosities, shapes, sizes, and spatial arrangements in multiple length scales. However, other classes of templates have been used to create particles by CVD polymerization. For example, Begum et al. reported that xylene radicals can diffuse into nanochannels of crystalline HKUST-1 metal-organic framework (MOF) during the CVD process, and upon removal of the coordinating metal ions, solid or porous PPX particles can be obtained depending on the precursor chemistry.[96] Cross-sectioned images of MOF via focused ion beam revealed that PPX particles fabricated using unsubstituted precursor (PCP-N) display a solid core whereas hollow-core particles were observed with 4-chloro[2.2]paracyclophane (PCP-C) precursors. This result suggests that PCP-N molecules can readily penetrate the whole micrometer scale MOF crystals, whereas polymerization of PCP-C was confined in the outer layer of the MOF due to a possible diffusion barrier. To

This article is protected by copyright. All rights reserved.

Author Manuscript

observe the difference in diffusivity of the two molecules, classical molecular dynamics simulations were performed. It was reported that the PCP-N monomer can easily diffuse to the neighboring pore of the MOF crystal within 3.7 ns whereas the PCP-C monomer required 170 ns because of the larger size of the monomer due to the presence of chlorine. Because of the slower diffusion rate of the PCP-C monomer, polymerization is confined to the first few layers of the MOF surface, resulting in hollow core particles. This study opens a new pathway toward the predictive design of polymeric particles by tethering precursor chemistry with the physical properties of the sacrificial template.

6. Conclusions and Technological Outlook

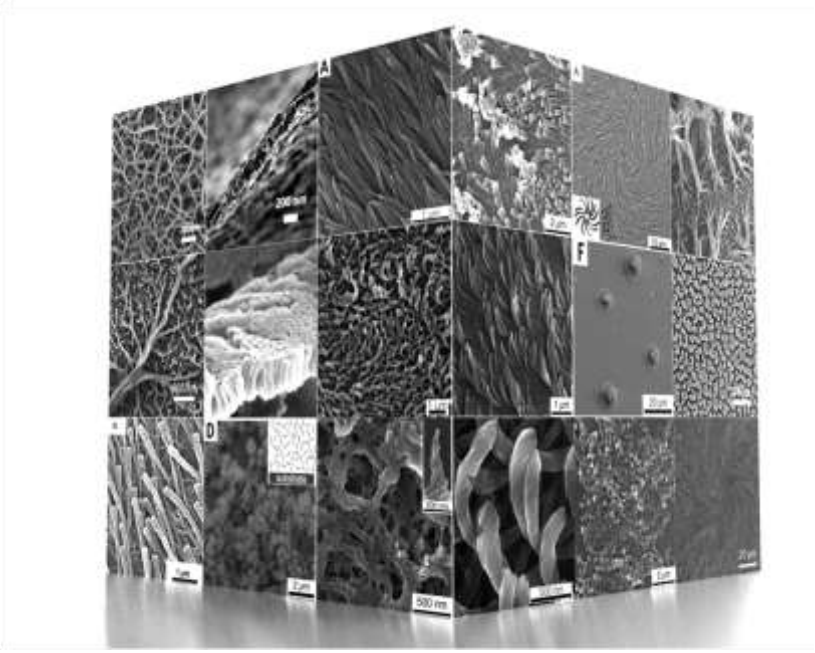


Figure 7. A collage of tailored morphologies of nanofiber array fabricated by LC-templated CVD polymerization. Reproduced with permission. [63] Copyright 2018, American Association for the Advancement of Science, [70] copyright 2022, Wiley-VCH, [81] copyright 2022, Wiley-VCH, [90] copyright 2023, American Chemical Society.

This article is protected by copyright. All rights reserved.

Author Manuscript

As outlined in this perspective, PPX can offer a unique combination of properties as dielectric layers and insulating coatings: they are chemically stable and tend to form defect-free barriers with excellent adhesion to the semiconductor layers. The seamless integration with other materials is critical for high charge mobility and extended stability. However, PPX coatings tend to feature lower dielectric constants than conventional SiOx materials. Also, PPX coatings are less established for use in FTEs and the long-term effects of CVD processing parameters on device performance are still not clearly understood. For membrane applications, PPX coatings offer tailor-made modifications that can be easily implemented through the choice of precursor and the control of coating thickness. Related to gas permeability, excellent selectivity has been reported for certain PPX coatings, but commercialization beyond specialty applications has been challenged by difficulties in scaling up the CVD process to an industrial scale that is commensurate with membrane applications. PPX coatings have sparked significant enthusiasm for biomedical coating applications because they offer versatile routes for the covalent attachment of biomolecules. However, functionalized precursors may require custom synthesis and, in spite of the relatively small amount of precursor needed for CVD polymerization, may add significant cost. PPX polymers are chemically inert, temperature stable, and resistant against solvents. This makes them ideal barrier coatings for a wide range of applications. However, depending on the functional site groups, PPX coatings are chemically reactive. In this case, their chemical and thermal stability may vary and some of these reactive coatings may age over time.[97]

Recent advances related to the use of templating phases for CVD polymerization have opened the door to achieving a hierarchy of morphologies, both at the nanoscale and mesoscale.[98,99] The unique advantage of using LC-templated CVD in comparison with the other conventional processes to fabricate fibrous structures (Table 1) is the modular nature of the approach – distinct phases of LC generate distinct morphologies. This approach leads to surfaces decorated with a range of three-dimensional polymeric nanostructures with diverse chemistries and functional properties, thus expanding greatly the opportunity to use PPX in contexts beyond planar films. By employing additional classes of templates, we envisage CVD polymerization yielding an expanded range of PPX nanostructures with

This article is protected by copyright. All rights reserved.

Author Manuscript

application in technologies such as biomedical devices (Figure 8). However, there are challenges associated with the use of PPXs that need to be solved in the future to realize an even broader applicability. Existing PPX coatings consist of high-molecular-weight polymers that cannot be depolymerized to the precursor state, which, if possible, would make the process more sustainable. Recent advances by Xie et al. showed that co-polymerization with 5,6-benzo-2-methylene-1,3-dioxepane monomers can yield ester linkages in the polymeric backbone, which are susceptible to hydrolytic degradation.[100] The degradability of the coatings makes them potentially interesting for applications such as biodegradable coating of stents or scaffolds for regenerative medicine.

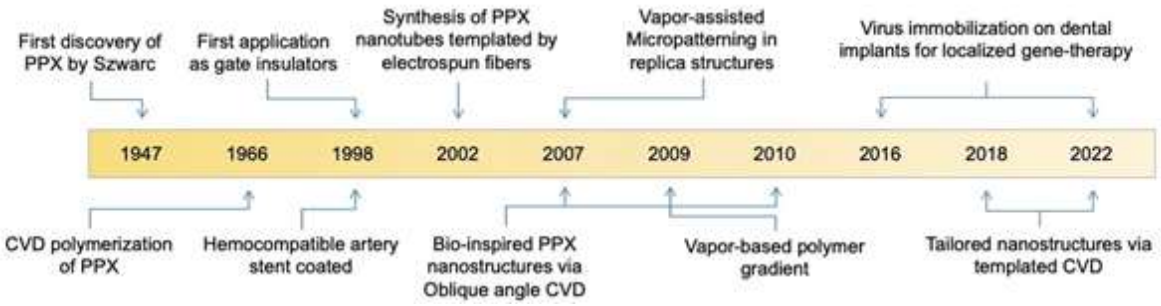


Figure 8. Timeline of the representative development in CVD polymerization of functionalized [2.2]paracyclophanes.

The synthesis of parylene precursors for CVD polymerization typically involves extensive wet chemistry with multiple synthesis and separation steps, which makes the process complex and time-consuming. Additionally, the range of monomer chemistries and side functional groups that are compatible with CVD polymerization is limited to functional PCP precursors. One of the current approaches to circumvent this problem is the post-modification of functional PPX coatings via reactions with functional groups introduced into the PCP precursors.[48,101,102] Additionally, there are constraints on the types of substrates that can be used for CVD due to the exposure of a substrate to a vacuum during deposition. Water-containing materials such as biological tissues cannot be coated, as the low pressure inside the CVD chamber removes the water. To mitigate this problem, a custom-built reactor

This article is protected by copyright. All rights reserved.

Author Manuscript

system could be developed that enables CVD polymerization in the presence of high-water vapor pressure despite the higher rate of collision of polar water molecules with the precursor radicals. Future research will likely expand the synthetic capabilities of CVD polymerization, and expand the range and scale of available polymer coatings. Beyond advances related to chemical and biological control of surfaces, templated CVD polymerization offers a scalable and robust route to topographically controlled polymer coatings that will likely find applications in optical components, medical devices and electronic applications. In addition, tailor-made solutions in diverse applications along with the recent advances in controlling the coating morphology and architecture make the CVD deposition process of [2.2]paracyclophanes a technologically important and scientifically rich topic deserving of further exploration.

Acknowledgements

This work has been in part supported by the Advanced Manufacturing Program of the National Science Foundation through Grants 2322900 (J. Lahann) and 2322899 (N. Abbott).

Received: ((will be filled in by the editorial staff))
Revised: ((will be filled in by the editorial staff))
Published online: ((will be filled in by the editorial staff))

[1] T. Moss, A. Greiner, *Adv Mater Interfaces* **2020**, *7*, 1901858.

[2] H. G. Gilch, W. L. Wheelwright, *J Polym Sci A1* **1966**, *4*, 1337.

[3] J. B. Fortin, T.-M. Lu, *Chemistry of Materials* **2002**, *14*, 1945.

[4] A. S. Mitko, D. R. Streltsov, P. V Dmitryakov, A. A. Nesmelov, A. I. Buzin, S. N. Chvalun, *Polymer Science, Series A* **2019**, *61*, 555.

[5] X. Deng, J. Lahann, *J Appl Polym Sci* **2014**, *131*.

[6] S. M. George, *Chem Rev* **2010**, *110*, 111.

[7] Z. Wang, Z. Zhang, In *Advanced Nano Deposition Methods*, **2016**, pp. 33--58.

This article is protected by copyright. All rights reserved.

Author Manuscript

[8] W. E. Tenhaeff, K. K. Gleason, *Adv Funct Mater* **2008**, *18*, 979.

[9] M. E. Alf, A. Asatekin, M. C. Barr, S. H. Baxamusa, H. Chelawat, G. Ozaydin-Ince, C. D. Petruczok, R. Sreenivasan, W. E. Tenhaeff, N. J. Trujillo, S. Vaddiraju, J. Xu, K. K. Gleason, *Advanced Materials* **2010**, *22*, 1993.

[10] R. M. Biefeld, *Materials Science and Engineering: R: Reports* **2002**, *36*, 105.

[11] Z. Hassan, E. Spuling, D. M. Knoll, J. Lahann, S. Bräse, *Chem Soc Rev* **2018**, *47*, 6947.

[12] M. Kreis, M. Nieger, S. Bräse, *J Organomet Chem* **2006**, *691*, 2171.

[13] Z. Hassan, D. Varadharajan, C. Zippel, S. Begum, J. Lahann, S. Bräse, *Advanced Materials* **2022**, *34*, 2201761.

[14] A. Asatekin, M. C. Barr, S. H. Baxamusa, K. K. S. Lau, W. Tenhaeff, J. Xu, K. K. Gleason, *Materials Today* **2010**, *13*, 26.

[15] M. SZWARC, *Nature* **1947**, *160*, 403.

[16] W. F. Gorham, *J Polym Sci A1* **1966**, *4*, 3027.

[17] C. A. Coulson, D. P. Craig, A. Maccoll, A. Pullman, *Discuss Faraday Soc* **1947**, *2*, 36.

[18] T. Yamada, M. Ishihara, J. Kim, M. Hasegawa, S. Iijima, *Carbon N Y* **2012**, *50*, 2615.

[19] T. Onoue, I. Nakamura, Y. Sakabe, T. Yasuda, T. Tsutsui, *Jpn J Appl Phys* **2006**, *45*, L770.

[20] T. Yasuda, K. Fujita, H. Nakashima, T. Tsutsui, *Jpn J Appl Phys* **2003**, *42*, 6614.

[21] B. J. Kim, E. Meng, *Polym Adv Technol* **2016**, *27*, 564.

[22] J. Lahann, *Polym Int* **2006**, *55*, 1361.

[23] J. P. Seymour, Y. M. Elkasabi, H.-Y. Chen, J. Lahann, D. R. Kipke, *Biomaterials* **2009**, *30*, 6158.

[24] S. Yang, K. Liu, Y. Xu, L. Liu, H. Li, T. Zhai, *Advanced Materials* **2023**, *35*, 2207901.

[25] C. D. Dimitrakopoulos, B. K. Furman, T. Graham, S. Hegde, S. Purushothaman, *Synth Met* **1998**, *92*, 47.

[26] T. E. Taouririt, A. Meftah, N. Sengouga, *Appl Nanosci* **2018**, *8*, 1865.

[27] J. Kim, S. C. Jang, K. Bae, J. Park, H.-D. Kim, J. Lahann, H.-S. Kim, K. J. Lee, *ACS Appl Mater Interfaces* **2021**, *13*, 43123.

This article is protected by copyright. All rights reserved.

Author Manuscript

[28] G. Maggioni, A. Campagnaro, S. Carturan, A. Quaranta, *Solar Energy Materials and Solar Cells* **2013**, *108*, 27.

[29] M. S. Kim, D.-H. Lee, H. J. Cho, J. Oh, S. Y. Lee, J. M. Kim, K. Park, Y.-S. Kim, *Org Electron* **2018**, *52*, 295.

[30] J. Zhao, W. Tang, Q. Li, W. Liu, X. Guo, *IEEE Electron Device Letters* **2017**, *38*, 1465.

[31] K. Fukuda, T. Suzuki, T. Kobayashi, D. Kumaki, S. Tokito, *physica status solidi (a)* **2013**, *210*, 839.

[32] H. Park, H. Ahn, J. Kwon, S. Kim, S. Jung, *ACS Appl Mater Interfaces* **2018**, *10*, 37767.

[33] H. Park, J. Kwon, H. Ahn, S. Jung, *J Mater Chem C Mater* **2019**, *7*, 6251.

[34] C. J. Lee, *Solid State Technology*. 2008, p. 28+.

[35] A. Abizaid, J. R. Costa, *Circ Cardiovasc Interv* **2010**, *3*, 384.

[36] G. Theocharidis, H. Yuk, H. Roh, L. Wang, I. Mezghani, J. Wu, A. Kafanas, M. Contreras, B. Sumpio, Z. Li, E. Wang, L. Chen, C. F. Guo, N. Jayaswal, X.-L. Katopodi, N. Kalavros, C. S. Nabzdyk, I. S. Vlachos, A. Veves, X. Zhao, *Nat Biomed Eng* **2022**, *6*, 1118.

[37] J. Zhu, H. Zhou, E. M. Gerhard, S. Zhang, F. I. Parra Rodríguez, T. Pan, H. Yang, Y. Lin, J. Yang, H. Cheng, *Bioact Mater* **2023**, *19*, 360.

[38] N. Li, Y. Li, Z. Cheng, Y. Liu, Y. Dai, S. Kang, S. Li, N. Shan, S. Wai, A. Ziaja, Y. Wang, J. Strzalka, W. Liu, C. Zhang, X. Gu, J. A. Hubbell, B. Tian, S. Wang, *Science (1979)* **2023**, *381*, 686.

[39] J. Hao, K. C. K. Cheng, L. G. Kruger, L. Larsson, J. V Sugai, J. Lahann, W. V Giannobile, *Advanced Materials* **2016**, *28*, 3145.

[40] Y. Zhang, X. Deng, E. L. Scheller, T.-G. Kwon, J. Lahann, R. T. Franceschi, P. H. Krebsbach, *Biomaterials* **2010**, *31*, 3231.

[41] J. A. Horowitz, X. Zhong, S. J. DePalma, M. R. Ward Rashidi, B. M. Baker, J. Lahann, S. R. Forrest, *Langmuir* **2021**, *37*, 1874.

[42] S. Maekawa, Y.-D. Cho, F. Kauffmann, Y. Yao, J. V Sugai, X. Zhong, C. Schmiedeler, N. Kinra, A. Moy, L. Larsson, J. Lahann, W. V Giannobile, *Adv Mater Interfaces* **2022**, *9*, 2200531.

[43] K. Schürmann, J. Lahann, P. Niggemann, B. Klosterhalfen, J. Meyer, A. Kulisch, D. Klee, R. W. Günther, D. Vorwerk, *Radiology* **2004**, *230*, 151.

This article is protected by copyright. All rights reserved.

Author Manuscript

[44] S. P. Pilipchuk, T. Fretwurst, N. Yu, L. Larsson, N. M. Kavanagh, F. Asa'ad, K. C. K. Cheng, J. Lahann, W. V Giannobile, *Adv Healthc Mater* **2018**, *7*, 1800750.

[45] T. Y. Chang, V. G. Yadav, S. De Leo, A. Mohedas, B. Rajalingam, C.-L. Chen, S. Selvarasah, M. R. Dokmeci, A. Khademhosseini, *Langmuir* **2007**, *23*, 11718.

[46] J. E. Puskas, L. G. Muñoz-Robledo, R. A. Hoerr, J. Foley, S. P. Schmidt, M. Evancho-Chapman, J. Dong, C. Frethem, G. Haugstad, *WIREs Nanomedicine and Nanobiotechnology* **2009**, *1*, 451.

[47] H. Nandivada, H.-Y. Chen, J. Lahann, *Macromol Rapid Commun* **2005**, *26*, 1794.

[48] F. Bally, K. Cheng, H. Nandivada, X. Deng, A. M. Ross, A. Panades, J. Lahann, *ACS Appl Mater Interfaces* **2013**, *5*, 9262.

[49] N. An, C. H. Zhou, X. Y. Zhuang, D. S. Tong, W. H. Yu, *Appl Clay Sci* **2015**, *114*, 283.

[50] J. Wan, L. Zhang, B. Yang, B. Jia, J. Yang, X. Su, *Chemical Engineering Journal* **2022**, *427*, 131976.

[51] H. S. Mansur, R. L. Oréfice, W. L. Vasconcelos, Z. P. Lobato, L. J. C. Machado, *J Mater Sci Mater Med* **2005**, *16*, 333.

[52] R. Kumar, J. Lahann, *ACS Appl Mater Interfaces* **2016**, *8*, 16595.

[53] R. Kumar, A. Welle, F. Becker, I. Kopyeva, J. Lahann, *ACS Appl Mater Interfaces* **2018**, *10*, 31965.

[54] J. Lahann, W. Plüster, D. Klee, H.-G. Gattner, H. Höcker, *J Mater Sci Mater Med* **2001**, *12*, 807.

[55] E. Manickan, J. S. Smith, J. Tian, T. L. Eggerman, J. N. Lozier, J. Muller, A. P. Byrnes, *Molecular Therapy* **2006**, *13*, 108.

[56] C. A. Dunn, Q. Jin, M. Taba, R. T. Franceschi, R. Bruce Rutherford, W. V Giannobile, *Molecular Therapy* **2005**, *11*, 294.

[57] H. Hopf, *Angewandte Chemie International Edition* **2008**, *47*, 9808.

[58] T. Shii, M. Hatori, K. Yokota, Y. Hattori, M. Kimura, *Sci Rep* **2017**, *7*, 15596.

[59] A. Tuteja, W. Choi, M. Ma, J. M. Mabry, S. A. Mazzella, G. C. Rutledge, G. H. McKinley, R. E. Cohen, *Science (1979)* **2007**, *318*, 1618.

[60] P. Vandezande, L. E. M. Gevers, I. F. J. Vankelecom, *Chem Soc Rev* **2008**, *37*, 365.

This article is protected by copyright. All rights reserved.

Author Manuscript

[61] S. Yoshida, T. Shii, Y. Kitazawa, M. L. Kim, E. H. Otal, Y. Hattori, M. Kimura, *Polymers (Basel)* **2023**, *15*.

[62] H.-Y. Chen, J. Lahann, *Advanced Materials* **2007**, *19*, 3801.

[63] K. C. K. Cheng, M. A. Bedolla-Pantoja, Y.-K. Kim, J. V Gregory, F. Xie, A. de France, C. Hussal, K. Sun, N. L. Abbott, J. Lahann, *Science (1979)* **2018**, *362*, 804.

[64] Z. Lei, Z. Li, M. Guo, P. Li, T. Da, S. Wang, Y. Wu, Y. He, J. Chen, *Compos B Eng* **2020**, *199*, 108286.

[65] Z. Liu, J. Lyu, D. Fang, X. Zhang, *ACS Nano* **2019**, *13*, 5703.

[66] G.-F. Liu, D. Zhang, C.-L. Feng, *Angewandte Chemie International Edition* **2014**, *53*, 7789.

[67] D. Demus, In *Handbook of Liquid Crystals Set*, **1998**, pp. 133--187.

[68] D. S. Fudge, N. Levy, S. Chiu, J. M. Gosline, *Journal of Experimental Biology* **2005**, *208*, 4613.

[69] R. M. Erb, J. S. Sander, R. Grisch, A. R. Studart, *Nat Commun* **2013**, *4*, 1712.

[70] S. Roh, J. Kim, D. Varadharajan, J. Lahann, N. L. Abbott, *Adv Funct Mater* **2022**, *32*, 2200830.

[71] K. Nayani, P. Rai, N. Bao, H. Yu, M. Mavrikakis, R. J. Twieg, N. L. Abbott, *Advanced Materials* **2018**, *30*, 1706707.

[72] E. Brasselet, N. Murazawa, H. Misawa, S. Juodkazis, *Phys Rev Lett* **2009**, *103*, 103903.

[73] E. Brasselet, *Phys Rev Lett* **2012**, *108*, 87801.

[74] Y. Zhang, P. Chen, L. Jiang, W. Hu, M. Liu, *J Am Chem Soc* **2009**, *131*, 2756.

[75] X. Feng, V. Marcon, W. Pisula, M. R. Hansen, J. Kirkpatrick, F. Grozema, D. Andrienko, K. Kremer, K. Müllen, *Nat Mater* **2009**, *8*, 421.

[76] Y. Yan, R. Wang, X. Qiu, Z. Wei, *J Am Chem Soc* **2010**, *132*, 12006.

[77] W. Zou, Y. Yan, J. Fang, Y. Yang, J. Liang, K. Deng, J. Yao, Z. Wei, *J Am Chem Soc* **2014**, *136*, 578.

[78] G. Yuan, K. Aruda, S. Zhou, A. Levine, J. Xie, D. Wang, *Angewandte Chemie International Edition* **2011**, *50*, 2334.

[79] P. Ringler, W. Müller, H. Ringsdorf, A. Brisson, *Chemistry -- A European Journal* **1997**, *3*, 620.

This article is protected by copyright. All rights reserved.

Author Manuscript

[80] E. M. Wilson-Kubalek, R. E. Brown, H. Celia, R. A. Milligan, *Proceedings of the National Academy of Sciences* **1998**, *95*, 8040.

[81] D. Varadharajan, K. Nayani, C. Zippel, E. Spuling, K. C. Cheng, S. Sarangarajan, S. Roh, J. Kim, V. Trouillet, S. Bräse, N. L. Abbott, J. Lahann, *Advanced Materials* **2022**, *34*, 2108386.

[82] M. Bognitzki, W. Czado, T. Frese, A. Schaper, M. Hellwig, M. Steinhart, A. Greiner, J. H. Wendorff, *Advanced Materials* **2001**, *13*, 70.

[83] L. Li, X. Zhang, Z. Zhang, M. Zhang, L. Cong, Y. Pan, S. Lin, *J Mater Chem A Mater* **2016**, *4*, 16635.

[84] Y.-C. Yoon, K.-S. Park, S.-D. Kim, *Thin Solid Films* **2015**, *597*, 125.

[85] S. Feng, R. Xu, *Acc Chem Res* **2001**, *34*, 239.

[86] S. Z. Qamar, A. F. M. Arif, A. K. Sheikh, *J Mater Process Technol* **2004**, *155--156*, 1734.

[87] S. Elgeti, M. Probst, C. Windeck, M. Behr, W. Michaeli, Ch. Hopmann, *Finite Elements in Analysis and Design* **2012**, *61*, 35.

[88] J. Yang, X. Zhen, B. Wang, X. Gao, Z. Ren, J. Wang, Y. Xie, J. Li, Q. Peng, K. Pu, Z. Li, *Nat Commun* **2018**, *9*, 840.

[89] S. Hirata, *Adv Opt Mater* **2017**, *5*, 1700116.

[90] M. Wawryszyn, R. Wilhelm, J. Kim, X. Zhong, J. E. Raymond, R. Thelen, V. Trouillet, M. Schwotzer, S. Bräse, D. H. Kim, N. L. Abbott, J. Lahann, *ACS Appl Polym Mater* **2023**, *5*, 1670.

[91] L. Gu, W. Ye, X. Liang, A. Lv, H. Ma, M. Singh, W. Jia, Z. Shen, Y. Guo, Y. Gao, H. Chen, D. Wang, Y. Wu, J. Liu, H. Wang, Y.-X. Zheng, Z. An, W. Huang, Y. Zhao, *J Am Chem Soc* **2021**, *143*, 18527.

[92] L. Zhang, M. Wei, L. Shao, M. Li, W. Dai, Y. Cui, Z. Li, C. Zhang, W. Wang, *Lab Chip* **2018**, *18*, 3539.

[93] L. Gu, H. Wu, H. Ma, W. Ye, W. Jia, H. Wang, H. Chen, N. Zhang, D. Wang, C. Qian, Z. An, W. Huang, Y. Zhao, *Nat Commun* **2020**, *11*, 944.

[94] Y.-M. Chang, J.-Q. Xiao, J. Christy, C.-Y. Wu, C.-W. Huang, T.-Y. Wu, Y.-C. Chiang, T.-H. Lin, H.-Y. Chen, *Mater Today Bio* **2022**, *16*, 100403.

[95] C.-Y. Wu, T.-Y. Wu, Z.-Y. Guan, P.-Y. Wang, Y.-C. Yang, C.-W. Huang, T.-H. Lin, H.-Y. Chen, *Nat Commun* **2021**, *12*, 3413.

This article is protected by copyright. All rights reserved.

Author Manuscript

[96] S. Begum, F. Behboodi-Sadabad, Y. Pramudya, C. Dolle, M. Kozlowska, Z. Hassan, C. Mattern, S. Gorji, S. Heißler, A. Welle, M. Koenig, W. Wenzel, Y. M. Eggeler, S. Bräse, J. Lahann, M. Tsotsalas, *Chemistry of Materials* **2022**, *34*, 6268.

[97] J. H.-C. Chang, Y. Liu, D. Kang, Y.-C. Tai, In *2013 Transducers & Eurosensors XXVII: The 17th International Conference on Solid-State Sensors, Actuators and Microsystems (TRANSDUCERS & EUROSENSORS XXVII)*, **2013**, pp. 2612--2615.

[98] G. Demirel, N. Malvadkar, M. C. Demirel, *Thin Solid Films* **2010**, *518*, 4252.

[99] N. A. Malvadkar, M. J. Hancock, K. Sekeroglu, W. J. Dressick, M. C. Demirel, *Nat Mater* **2010**, *9*, 1023.

[100] F. Xie, X. Deng, D. Kratzer, K. C. K. Cheng, C. Friedmann, S. Qi, L. Solorio, J. Lahann, *Angewandte Chemie International Edition* **2017**, *56*, 203.

[101] H. Nandivada, H.-Y. Chen, L. Bondarenko, J. Lahann, *Angewandte Chemie International Edition* **2006**, *45*, 3360.

[102] X. Deng, T. W. Eyster, Y. Elkasabi, J. Lahann, *Macromol Rapid Commun* **2012**, *33*, 640.



John Kim studied materials science and engineering and received B.S. at Sungkyunkwan University in Republic of Korea. He is currently pursuing his Ph.D. in materials science and engineering at University of Michigan. His research focuses on the surface chemistry and engineering of functional nanofibers templated by liquid crystalline film using chemical vapor deposition.

This article is protected by copyright. All rights reserved.

Author Manuscript



Arit Patra received his Dual Degree Bachelor's and master's in chemical engineering from the Indian Institute of Technology, Kharagpur, India. He is pursuing his Ph.D. in the Department of Chemical Engineering at the University of Michigan, Ann Arbor. His current research focuses on the synthesis of paracyclophane-based polymeric nanofibers templated along the liquid crystalline defects.

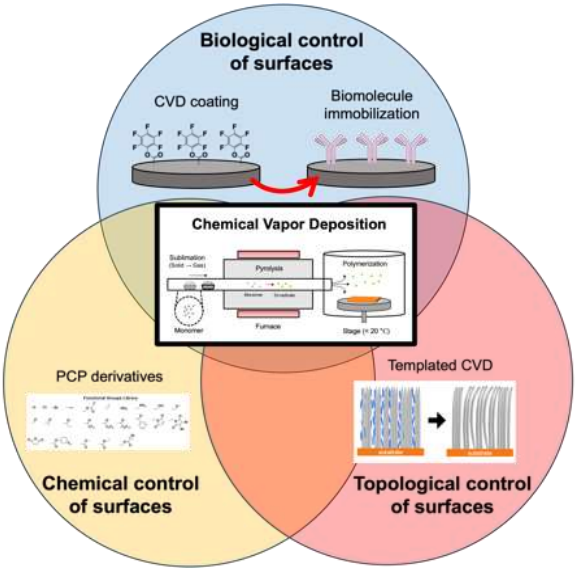


Soumyamouli Pal received his Bachelors of Technology (B. Tech) in Chemical Engineering at the Indian Institute of Technology (IIT) Kharagpur in India in 2019. He is currently pursuing his Ph.D. in Chemical and Biomolecular Engineering at Cornell University under the supervision of Prof. Nicholas L. Abbott. His research interests lie in areas involving liquid crystals and polymerization. His research is focused on fabrication of polymeric nanostructures via chemical vapor polymerization into liquid crystalline templates.

This article is protected by copyright. All rights reserved.

Author Manuscript

Table of contents



Chemical vapor deposition is an effective technique to control the chemical, biological, and topographical properties of surfaces. In this perspective, we highlight the CVD polymerization of [2.2]paracyclophanes and discuss emergent applications as electrical components, biological interfaces, and biomimetic nanostructures.

This article is protected by copyright. All rights reserved.